Astronomy Department Faculty Publication Series

Astronomy

2010

Testing Subhalo Abundance Matching in Cosmological Smoothed Particle Hydrodynamics Simulations

V Simha

D Weinberg

R Dave

M Fardal

N Katz
University of Massachusetts - Amherst, nsk@astro.umass.edu

See next page for additional authors

Recommended Citation

Authors

V Simha, D Weinberg, R Dave, M Fardal, N Katz, and B Oppenheimer

Testing Subhalo Abundance Matching in Cosmological Smoothed Particle Hydrodynamics Simulations

Vimal Simha[1], David H. Weinberg[1], Romeel Davé[2],
Mark Fardal[3], Neal Katz[3], Benjamin D. Oppenheimer[4]

[1] *Astronomy Department and Center for Cosmology and AstroParticle Physics, Ohio State University, Columbus, OH 43210,*
vsimha,dhw@astronomy.ohio-state.edu
[2] *University of Arizona, Steward Observatory, Tuscon, AZ 85721, rad@as.arizona.edu*
[3] *Astronomy Department, University of Massachusetts at Amherst, MA 01003, fardal,nsk@kaka.astro.umass.edu*
[4] *Leiden Observatory, Leiden University, 2300 RA Leiden, The Netherlands; oppenheimer@strw.leidenuniv.nl*

24 November 2010

ABSTRACT
Subhalo abundance matching (a.k.a. SHAM) is a technique for populating simulated dark matter distributions with galaxies, assuming a monotonic relation between a galaxy's stellar mass or luminosity and the mass of its parent dark matter halo or subhalo. We examine the accuracy of SHAM in two cosmological smoothed particle hydrodynamics (SPH) simulations, one of which includes momentum−driven galactic winds. The SPH simulations indeed show a nearly monotonic relation between stellar mass and halo mass provided that, for satellite galaxies, we use the mass of the subhalo at the epoch $z_{\rm sat}$ when it became a satellite. In each simulation, the median relation for central and satellite galaxies is nearly identical, though a somewhat larger fraction of satellites are outliers because of stellar mass loss. SHAM-assigned masses (at $z = 0 - 2$), luminosities (R-band at $z = 0$), or star formation rates (at $z = 2$) have a 68% scatter of $0.09 - 0.15$ dex relative to the true simulation values. When we apply SHAM to the subhalo population of a collisionless N-body simulation with the same initial conditions as the SPH runs, we find generally good agreement for the halo occupation distributions and halo radial profiles of galaxy samples defined by thresholds in stellar mass. However, because a small fraction of SPH galaxies suffer severe stellar mass loss after becoming satellites, SHAM slightly overpopulates high mass halos; this effect is more significant for the wind simulation, which produces galaxies that are less massive and more fragile. SHAM recovers the two-point correlation function of the SPH galaxies in the no-wind simulation to better than 10% at scales $0.1h^{-1}{\rm Mpc} < r < 10h^{-1}{\rm Mpc}$. For the wind simulation, agreement is better than 15% at $r > 2h^{-1}{\rm Mpc}$, but overpopulation of massive halos increases the correlation function by a factor ~ 2.5 on small scales.

Key words: galaxies: evolution — galaxies: formation — models: semi-analytic — models: numerical

1 INTRODUCTION

In the standard theoretical description of galaxy formation, galaxies form by the dissipation of the baryonic component within collisionless dark matter halos (e.g. White & Rees 1978; Fall & Efstathiou 1980). When a dark matter halo enters the virial radius of a more massive halo, it is subjected to tidal stripping and potentially to disruption. Nonetheless, high resolution N-body simulations have indicated that massive halos retain a substantial amount of substructure (Klypin et al. 1999; Moore et al. 1999; Springel et al. 2001), consisting of bound dark matter clumps orbiting within the

potential of their host halo. Evidently, such subhalos were themselves independent, self-contained halos in the past, before merging with a more massive halo. If sufficiently massive, these subhalos were sites of baryon dissipation and star formation in the past. There are many indications from studies of the statistical properties of how galaxies and substructures populate halos that galaxies in groups and clusters are in fact the observational counterparts of subhalos. For example, Colín et al. (1999) and Kravtsov et al. (2004) show that the correlation functions of substructures in high resoution N-body simulations are in good agreement with

the observed correlation functions of galaxies. On the theory side, Kravtsov et al. (2004) find that the distribution of subhalos in high resolution N-body simulations is similar to that of smoothed particle hydrodynamics (SPH) galaxies in Berlind et al. (2003) and Zheng et al. (2005).

Subhalo abundance matching (SHAM) is a technique for assigning observable galaxy properties to a halo/subhalo population in an N-body simulation. It is based on assuming a monotonic relationship between observable properties of galaxies and dynamical properties of dark matter substructures. As subhalos that fall into the virial radius of more massive halos are subjected to stripping and tidal disruption, several authors (e.g. Conroy et al. 2006; Vale & Ostriker 2006; Moster et al. 2010) contend that the properties of satellite galaxies should be better correlated with the properties of subhalos at the time of their accretion onto a more massive halo rather than their present day properties. By using the SHAM technique, with this accretion-epoch matching, Conroy et al. (2006) match the observed luminosity dependence of galaxy clustering at a wide range of epochs, ranging from $z = 0$ to $z \sim 5$. Assuming a monotonic relationship between galaxy mass and halo mass and using the same SHAM technique, Guo et al. (2010) reproduce the observationally inferred relation between stellar mass and halo virial mass. Trujillo-Gomez et al. (2010) use the abundance matching technique to match the observed relations between stellar mass and circular velocity and luminosity and circular velocity, and to match the estimated galaxy velocity function.

In this paper, we investigate the effectiveness of subhalo abundance matching (SHAM) in cosmological SPH simulations, where we know exactly the relation between the properties of galaxies and the masses of their parent halos and subhlaos. We investigate the degree to which there is a direct correspondence between the properties of dark matter substructures in a dissipationless numerical simulation of a cosmological volume and condensed baryons in numerical simulations (with the same initial conditions) that include a dissipative component. We extend the similar study of Weinberg et al. (2008) in several ways. Firstly, our simulation volume is more than ten times larger. Secondly, one of our dissipative simulations includes ejective feedback in the form of momentum driven winds, which curtail star formation and produces a stellar mass function that is in better agreement with the observations. Lastly and perhaps most importantly, we relate galaxy properties to the subhalo mass at the epoch of accretion rather than at the present time (see comparison in §4). We make a direct assessment of the effectiveness of SHAM as a method for assigning stellar mass, luminosity or star formation rate to subhalos and investigate the sources of its breakdown.

Our investigation offers insight into the physical mechanisms that shape galaxy masses and luminosities in these simulations, and it also has practical import. If the subhalo population in the purely gravitational simulation does indeed trace the observable properties of the galaxy population, it enables us to make observable predictions of quantities like the luminosity dependence of galaxy clustering based on computationally less expensive N-body simulations instead of hydrodynamic simulations. SHAM also offers a relatively inexpensive tool for creating artificial galaxy catalogues to support statistical analyses of large scale structure data sets.

In §2, we describe our simulation, method for identifying halos, subhalos and galaxies, and the subhalo abundance matching scheme. In §3, we investigate the relationship between the stellar masses, luminosities, and star formation rates of SPH galaxies and dark matter substructures in our SPH simulations to test some of the underlying assumptions of the subhalo abundance matching technique. In §4, we investigate whether the SPH galaxy population can be recovered from the subhalo population in our matched N-body simulation; note that it is this comparison rather than the investigations in §3 that tests SHAM as it has been traditionally implemented. Finally, in §5, we summarise our results and discuss their implications.

2   METHODS

2.1   Simulations

Our simulations are performed using the GADGET-2 code (Springel 2005) as modified by Oppenheimer & Davé (2008). Gravitational forces are calculated using a combination of the Particle Mesh algorithm (Hockney & Eastwood 1981) for large distances and the hierarchical tree algorithm (Barnes & Hut 1986; Hernquist 1987) for short distances. The smoothed particle hydrodynamics (SPH) algorithm is entropy and energy conserving and is based on Springel & Hernquist (2002). The details of the treatment of radiative cooling can be found in Katz, Weinberg & Hernquist (1996). Gas can dissipate energy via Compton cooling and radiative cooling, computed assuming a primordial gas composition and a background UV flux based on Haardt & Madau (2001). The details of the treatment of star formation can be found in Springel & Hernquist (2003). Briefly, each gas particle satisfying a temperature and density criterion is assigned a star formation rate, but the conversion of gaseous material to stellar material proceeds stochastically. The parameters for the star formation model are selected so as to match the $z = 0$ relation between star formation rate and gas density (Kennicutt 1998; Schmidt 1959).

We adopt a ΛCDM cosmology (inflationary cold dark matter with a cosmological constant) with $\Omega_m = 0.25$, $\Omega_\Lambda = 0.75$, $h \equiv H_0/100$ km s^{-1}Mpc^{-1}=0.7, $\Omega_b = 0.044$, spectral index $n_s = 0.95$, and the amplitude of the mass fluctuations scaled to $\sigma_8 = 0.8$. These values are reasonably close to current estimates from the cosmic microwave background (Larson et al. 2010) and large scale structure (Reid et al. 2010). We do not expect minor changes in the values of the cosmological parameters to affect our conclusions.

We follow the evolution of 288^3 dark-matter particles and 288^3 gas particles, i.e. just under 50 million particles in total, in a comoving box that is $50h^{-1}$ Mpc on each side, from $z = 129$ to $z = 0$. The dark matter particle mass is 4.3×10^8 $M_\odot$, and the SPH particle mass is 9.1×10^7 $M_\odot$. The gravitational force softening is a comoving $5h^{-1}$ kpc cubic spline, which is roughly equivalent to a Plummer force softening of $3.5h^{-1}$ kpc.

One of our simulations, SPHw (SPH winds) incorporates kinetic feedback through momentum driven

winds as implemented by Oppenheimer & Davé (2006) and Oppenheimer & Davé (2008) where the details of the implementation can be found. Briefly, wind velocity is proportional to the velocity dispersion of the galactic halo, and the ratio of the gas ejection rate to the star formation rate is inversely proportional to the velocity dispersion of the galactic halo.

We also carry out a simulation with the same cosmological and numerical parameters as the SPHw simulation, but without momentum driven winds, SPHnw (SPH No Winds). Although no energy is kinetically imparted to SPH particles, the SPHnw simulation includes thermal feedback from supernovae (see Springel & Hernquist 2003). However, since the surrounding gas is dense, the energy is radiated away before it can drive outflows or significantly suppress star formation. Our SPHnw and SPHw simulations are analogous to the nw and vzw simulations of Oppenheimer et al. (2010), who investigate the growth of galaxies by accretion and wind recycling and compare predicted mass functions to observations. Our simulations are also used by Zu et al. (2010), who investigate intergalactic dust extinction.

In addition to the two SPH simulations, we carry out a non-dissipative, purely gravitational, N-body simulation with identical cosmological and numerical parameters and the same initial positions and velocities of particles as the SPH simulations, except that the dark matter particle mass is higher by a factor of $\Omega_m/(\Omega_m - \Omega_b)$ to compensate for the gravitational effects of not including baryons. We refer to this N-body simulation as the DM (dark matter only) simulation.

2.2 Identification of Groups and Substructures

We identify dark matter haloes using a FOF (friends-of-friends) algorithm (Davis et al. 1985). The algorithm selects groups of particles in which each particle has at least one neighbour within a linking length. We assign a mass to the halos using a SO (spherical overdensity) criterion, with the threshold density set to the virial overdensity in spherical collapse (Kitayama & Suto 1996). At $z = 0$, the mean interior overdensity is 94. We set the centre of the group at the most bound FOF particle and go out in radius until the mean density enclosed is equal to the virial density.

To identify substructures within halos, we use the publicly available code AdaptaHOP (Aubert et al. 2004). The details of the algorithm can be found in Aubert et al. (2004). Basically, it involves using an SPH-like kernel to compute densities at the location of each particle and partitioning the ensemble of particles into subhalos based on saddle points in the density field.

Hydrodynamic cosmological simulations that incorporate cooling and star formation produce dense groups of baryons with sizes and masses comparable to the luminous regions of observed galaxies (Katz 1992; Evrard et al. 1994). We identify galaxies using the Spline Kernel Interpolative DENMAX (SKID[1]) algorithm (Gelb & Bertschinger 1994; Katz, Weinberg & Hernquist 1996), which identifies gravitationally bound particles associated with a common density maximum. We refer to the groups of stars and cold gas

thus identified as galaxies. The simulated galaxy population becomes substantially incomplete below our resolution threshold of ~ 64 SPH particles (Murali et al. 2002), which corresponds to a baryonic mass of $5.8 \times 10^9 \ M_\odot$. Although this threshold applies to the total baryonic mass (stars plus cold, dense gas) of galaxies, we adopt it as our threshold for stellar mass and ignore galaxies with lower stellar mass.

Figure 1 compares the galaxy stellar mass function in the SPHnw and SPHw simulations at $z = 0$. In the SPHnw simulation, there are 7,952 galaxies above our resolution threshold, corresponding to a space density of 0.064 h^3 Mpc^{-3}. In the SPHw simulation there are only 2,264 galaxies above our resolution threshold, corresponding to a space density of 0.018 h^3 Mpc^{-3} because wind feedback pushes the stellar mass of many galaxies below the 64 m$_{\rm SPH}$ threshold. The two mass functions gradually converge towards higher masses, joining at $M_S > 10^{11.8}$ M$_\odot$, because wind feedback has less suppressing effect in larger systems since the amount of material ejected in this model scales inversely with circular velocity. Oppenheimer et al. (2010) discuss the comparison between the predicted stellar mass functions and observational estimates in some detail. Roughly speaking, the SPHw model reproduces observational estimates for $M_S < 10^{11}$ M$_\odot$, but it predicts excessive galaxy masses (at a given space density) for $M_g > 10^{11.8}$ M$_\odot$.

2.3 Subhalo Abundance Matching

Subhalo abundance matching (SHAM) is a technique for assigning galaxies to simulated dark matter halos and subhalos. The essential assumptions are that all galaxies reside in identifiable dark matter substructures and that luminosity or stellar mass of a galaxy is monotonically related to the potential well depth of its host halo or subhalo. Some implementations use the maximum of the circular velocity profile as the indicator of potential well depth, while others use halo or subhalo mass. The first clear formulations of SHAM as a systematic method appear in Conroy et al. (2006) and Vale & Ostriker (2006), but these build on a number of previous studies that either test the underpinnings of SHAM or implicitly assume SHAM-like galaxy assignment (e.g. Colín et al. 1999; Kravtsov et al. 2004; Nagai & Kravtsov 2005).

N-body simulations produce subhalos that are located within the virial radius of SO halos. The present mass of subhalos is a product of mass build up during the period when the halo evolves in isolation and tidal mass loss after it enters the virial radius of a more massive halo (e.g. Kravtsov et al. 2004; Kazantzidis et al. 2004). The stellar component, however, is at the bottom of the potential well and more tightly bound making it less likely to be affected by tidal forces. Therefore, several authors (e.g. Conroy et al. 2006; Vale & Ostriker 2006) argue that the properties of the stellar component should be more strongly correlated with the subhalo mass at the epoch of accretion rather than at $z = 0$.

Vale & Ostriker (2006) apply a global statistical correction to subhalo masses relative to halo masses (as do Weinberg et al. 2008), while Conroy et al. (2006) explicitly identify subhalos at the epoch of accretion and use the maximum circular velocity at that epoch. Our formulation here is similar to that of Conroy et al. (2006), though we use mass

---

[1] http://www-hpcc.astro.washington.edu/tools/skid.html

rather than circular velocity. Specifically, we assume a monotonic relationship between stellar mass and halo mass and determine the form of this relation by solving the implicit equation

$$n_S(> M_S) = n_H(> M_H), \quad (1)$$

where n_S and n_H are the number densities of galaxies and halos, respectively, M_S is the galaxy stellar mass threshold, and M_H is the halo mass threshold chosen so that the number density of halos above it is equal to the number density of galaxies in the sample. The quantity M_H is defined as follows:

$$M_H = \begin{cases} M_{\mathrm{halo}}(z=0) & \text{for distinct halos,} \\ M_{\mathrm{halo}}(z=z_{\mathrm{sat}}) & \text{for subhalos,} \end{cases} \quad (2)$$

where z_{sat} is the epoch when a halo first enters the virial radius of a more massive halo.

In §3, we use our SPH simulations to test the degree to which galaxy stellar mass and luminosity are monotonic functions of halo/subhalo mass, as assumed in SHAM. For independent halos, we set M_H equal to the $z = 0$ mass of SO halos. We use the AdaptaHOP code to identify subhalos hosting satellite galaxies above the resolution threshold at $z = 0$ in our SPH simulations. We then use their particle membership to identify their progenitor SO halos at z_{sat}, whose mass we adopt as M_H. We can identify a host subhalo for the vast majority of our galaxies at $z = 0$. However, for about one percent of galaxies we cannot identify any associated substructure. In these cases, we use the galaxy's baryonic particles to trace its high redshift progenitors up to the epoch when it was the only galaxy in a SO halo and adopt the mass of this SO halo as M_H. After matching, we examine the correlations of galaxy properties with M_H for both central and satellite systems, and we compare the stellar masses, luminosities, and (at high redshift) star formation rates that would be assigned by monotonic matching to the simulation values. Of course, SHAM is usually applied to collisionless N-body simulations, not SPH simulations, and the subhalo populations can differ even for the same initial conditions because of the dynamical effects of the dissipative baryons on the dark matter.

In §4, we populate halos/subhalos in our DM-only simulation using SHAM, following a procedure akin to the one usually used to match simulated halos/subhalos to observed galaxies. For independent halos, we set M_H equal to the $z = 0$ mass of SO halos. We identify subhalos using the AdaptaHOP code and use their particle membership to identify their progenitor SO halos at z_{sat}, whose mass we adopt as M_H. For comparison, we also implement a procedure that we refer to as SHAMz0, where we set M_H equal to the $z = 0$ mass for both independent halos and subhalos identified in our N-body simulation.

3   SHAM IN THE SPH SIMULATIONS

3.1   Stellar Mass

The left column of Figure 2 shows galaxy stellar mass plotted against halo mass in the SPHnw simulation (top) and the SPHw simulation (bottom). For galaxies that are the central objects of their parent halos (henceforth central galaxies),

the halo mass, M_H, on the horizontal axis, is the mass of the SO halo in which the galaxy is located at $z = 0$. For galaxies that are not the central objects of their respective SO halos (henceforth satellite galaxies), M_H is the mass of the SO halo in which the galaxy is located at z_{sat}, the last output epoch before its parent halo fell into the virial radius of a more massive halo; z_{sat} values range between $z = 3$ and $z = 0.05$. The black solid curve and red dotted curve show the median galaxy stellar mass in evenly spaced logarithmic bins of halo mass for all galaxies and satellite galaxies respectively, while the red open circles and black open rectangles show individual galaxies that are within the top five percent and bottom five percent by stellar mass in each halo mass bin.

The key result of Figure 2 is that the ratio of galaxy mass to M_H is similar for central galaxies and satellite galaxies. Between z_{sat} and $z = 0$, satellite galaxies have lower growth rates compared to central galaxies of similar mass (see Kereš et al. 2009; Simha et al. 2009). However, during the same time period, while central galaxies grow at a faster rate, their host halos also accrete mass and "receive" mergers of lower mass halos. The balance between stellar mass growth and halo mass growth leads to a similar M_S-M_H relation at $z = 0$ for central and satellite systems, in both simulations.

Note that in Figure 2 as well as in the remainder of this section, we only consider galaxies that are above our resolution threshold at $z = 0$, with $M_S > 64m_{\mathrm{SPH}} = 5.8 \times 10^9$ M$_\odot$. However, some satellite galaxies in dense environments experience mass loss between z_{sat} and $z = 0$, and, consequently, a fraction of satellites that are above the resolution threshold at z_{sat} are pushed below it by $z = 0$. We defer examination of this point to §4 (see Figure 11), where we show that it has a noticeable impact on the occupation of high mass halos in the SPHw simulation.

We assign galaxies to the halo/subhalo population via the monotonic mapping procedure described in §2. The right-hand side column of Figure 2 shows the distribution of the ratio of the stellar mass assigned to a halo to the stellar mass of the SPH galaxy that is actually located within it for the SPHnw simulation (top) and the SPHw simulation (bottom). In addition to the distribution for all galaxies (black solid curve), we show the distribution for satellite galaxies alone (red dotted curve). For most halos, the SHAM assigned mass is close to the mass of the SPH galaxy located within it in both the SPHnw and the SPHw simulations, although there are a small number of extreme outliers. We characterise the width of the distributions by σ_M such that 68% of galaxies have $|R| = |\log M_A/M_R| < \sigma_M$ where M_A is the assigned mass and M_R is the SPH (real) mass. In the SPHnw simulation, the width of the distribution is $\sigma_M = 0.09$, while in the SPHw simulation $\sigma_M = 0.11$. In both simulations, the distribution of SHAM assigned masses for satellite galaxies is also centered on the SPH mass, but there is greater scatter than in the case of central galaxies. For satellite galaxies in the SPHnw simulation, the distribution of assigned mass is skewed such that the assigned mass is likely to be slightly higher than the SPH mass.

Figure 3 presents the same distribution of $|\log M_A/M_R|$ at $z = 0.5, 1$ and 2, and compared to the $z = 0$ result from Figure 2. There is good agreement between the SHAM assigned stellar masses and the SPH stellar masses at all four

epochs. The fraction of satellite galaxies decreases with increasing redshift. Despite this, σ_M shows a continuous trend of increasing with redshift, from 0.09 at $z = 0$ to 0.13 at $z = 2$ in the SPHnw simulation, and from 0.11 at $z = 0$ to 0.14 at $z = 2$ in the SPHw simulation. Although the total baryonic mass (not shown) is equally well correlated with halo mass at $z = 2$ and at $z = 0$, the higher mean gas fraction and the larger halo-to-halo scatter in gas fraction at high redshift leads to higher scatter in the halo mass-stellar mass relation.

While the relationship between halo mass and galaxy stellar mass is roughly monotonic in our SPH simulations, there is some scatter, with the strongest outliers arising from satellite galaxies. We examine the sources of this scatter in Figure 4, both to understand the physical processes that give rise to it and to explore the possibility of adding a parameter that would sharpen the subhalo abundance matching. We restrict ourselves to $z = 0$ as the satellite galaxy sample is largest at this epoch. Each panel plots satellite galaxy stellar mass as a function of M_H at $z_{\rm sat}$ with SPHnw in the top panels and SPHw in the bottom.

In panel (a), points are colour coded by the mass of the $z = 0$ halo (not subhalo) that hosts the satellite, and lines show the median relation in each of the four halo mass bins. The median curves are nearly identical for the four bins, indicating that the typical M_S/M_H is at most minimally correlated with the final halo mass. The outlier points at low M_S/M_H are mostly galaxies that have experienced mass loss. These outliers are found in all $M_{\rm halo}$ bins; one should not read too much into the relative numbers of outlier points as the total number of satellites varies from bin to bin. We caution that this figure does not show galaxies that have fallen below the $M_S = 64 \ m_{\rm SPH}$ threshold by $z = 0$ (see Figure 11, below).

In panel (b), points and lines are coded by satellite accretion epoch. Once again, there is little difference in the median relations and outliers are found in all the $z_{\rm sat}$ bins (except $z_{\rm sat} > 2$). Panel(c) divides galaxies into those that have lost stellar mass since $z_{\rm sat}$, those that have increased their stellar mass by less than 10% since $z_{\rm sat}$ and those that have increased their stellar mass by more than 10%. Not surprisingly, galaxies that have lost stellar mass have systematically lower M_S/M_H at $z = 0$. Median relations for the other two populations are similar. There are some galaxies that are low M_S/M_H outliers despite having gained mass since $z_{\rm sat}$, indicating that at least some of this outlier population comes from satellites that had anomalously low M_S at $z_{\rm sat}$.

3.2 Luminosity and Star Formation Rate

So far, we have used SHAM to assign stellar masses to halos and compare them to the stellar masses of SPH galaxies located in those halos. However, when SHAM is applied to an observed galaxy population, it is often used to assign luminosities to simulated halos to compare the luminosity dependence of the clustering properties of the simulated halos to that of the observed galaxies.

The luminosity of a galaxy is correlated with its stellar mass, but is not reducible to a simple function of stellar mass because the stars formed at different times. We track the star formation histories of simulated galaxies in our SPH

simulations, and use the stellar population synthesis package of Conroy et al. (2009) to compute their luminosities. We assume that stars are formed with a Chabrier initial mass function. We assume solar metallicity and do not consider dust extinction. Changing the initial mass function in a uniform way would alter the zero-point of the luminosity-stellar mass relation but would not be likely to add scatter, while including dust extinction would shift the mean relation and increase the scatter somewhat.

The left column of Figure 5 shows the r-band luminosity of SPH galaxies against halo mass in the SPHnw simulation (top) and the SPHw simulation (bottom). For galaxies that are the central objects of their parent halos (henceforth central galaxies), the halo mass, M_H, on the horizontal axis, is the mass of the SO halo in which the galaxy is located at $z = 0$. For satellite galaxies, it is the mass of the SO halo in which the galaxy is located at $z_{\rm sat}$, the last output epoch before its parent halo fell into the virial radius of a more massive halo. The points show individual galaxies that are either in the top 5% or bottom 5% by luminosity in each halo mass bin. Most of the low luminosity outliers are satellite galaxies. This is primarily because satellite galaxies typically have an older stellar population than central galaxies of similar stellar mass and are, therefore, less luminous. A secondary factor, of less importance, is the difference between central and satellite galaxies in the stellar mass-halo mass relation shown in Figure 2. To assign luminosities to our halos, we rank order halos by mass and assign galaxies rank ordered by r-band luminosity to them. The right column of Figure 5 shows the distribution of the ratio of the SHAM assigned luminosity of a halo to the luminosity of the SPH galaxy within it in the SPHnw simulation (top right) and the SPHw simulation (bottom right). In both simulations, the distribution of SHAM assigned luminosities is centered on the SPH luminosity. In analogy with the previous subsection, we define σ_L such that 68% of galaxies have $|R| = |\log L_A/L_R| < \sigma_L$ where L_A is the assigned luminosity and L_R is the SPH (real) luminosity. In the SPHnw as well as the SPHw simulation, $\sigma_L = 0.15$, which is greater than the corresponding σ_M (see Figure 2). For satellite galaxies, the assigned luminosity is systematically higher than the SPH luminosity because of the stellar population differences, the offset being 0.08 dex in the SPHnw simulation but only 0.02 dex in the SPHw simulation.

The clustering properties of $z \geq 2$ galaxies are studied observationally using the Lyman break technique, in which high redshift star forming galaxies are identified by optical photometry alone using their redshifted rest frame UV radiation (Steidel et al. 1996, 1999, 2003). Conroy et al. (2006) find good agreement between the clustering of Lyman break galaxies (LBGs) and the clustering of halos in their N-body simulation when they use SHAM to match halos to galaxies. The relationship between LBGs and their host halos is important in understanding the properties of LBGs, in particular whether they are a quiescent star-forming population (Coles et al. 1998; Mo et al. 1999; Giavalisco & Dickinson 2001) or a merger driven starbust population (Somerville et al. 2001; Scannapieco & Thacker 2003).

In Figure 6, we investigate the relationship between the $z = 2$ star formation rates (SFRs) of SPH galaxies and the properties of their parent halos, in the same format used

previously for stellar mass and r-band luminosity at $z = 0$. In contrast to $z = 0$, where there is a significant passive, non star forming population, only ~ 0.1 % of galaxies have no star formation at $z = 2$, and these are excluded from the analysis. In the absence of dust extinction, the instantaneous SFR should be a good indicator of rest-frame UV luminosity, since the latter is dominated by the output of young, short-lived stars. We caution, however, that dust extinction corrections for LBG UV luminosities are typically factors of several (e.g. Steidel et al. 2003), and a scatter in extinction at fixed SFR could add significant scatter to the relation between M_H and UV luminosity. Since colours provide an indication of extinction, the most effective strategy for observational analysis is probably to apply colour based extinction corrections before subhalo abundance matching, so that only the errors in the corrections add scatter.

Figure 6 shows that the relation between intrinsic SFR and M_H at $z = 2$ is nearly as tight as the relation between R-band luminosity and M_H at $z = 0$. The 68% scatter of |log $\mathrm{SFR}_A/\mathrm{SFR}_R|$ is $\sigma_S = 0.12$ and $\sigma_S = 0.16$ for the SPHnw and SPHw simulations respectively, compared to the R-band luminosity scatters of $\sigma_L = 0.15$ for both simulations at $z = 0$. The median relations for central and satellite galaxies are nearly the same, in both cases, with offsets that are small compared to the intrinsic scatter. However, in the no-wind simulation the outliers at low SFR are preferentially satellites, a result of the gradual shutoff of gas accretion after galaxies become satellites in larger halos (Kereš et al. 2009; Simha et al. 2009). The $\mathrm{SFR}_A/\mathrm{SFR}_R$ histogram is, therefore, skewed towards overestimated SFRs for satellites, though this remains a small effect. For the wind simulation, there are many fewer galaxies above our 64 m_{SPH} stellar mass threshold, and star formation rates at $M_H < 10^{12.4}\mathrm{M}_\odot$ are suppressed by the momentum driven outflows. In this simulation, there are more satellite outliers at high SFR, and the (noisy) histogram of $\mathrm{SFR}_A/\mathrm{SFR}_R$ for satellite galaxies shows an overall shift toward underestimated SFR. For central galaxies, gas fractions in the SPHw simulation are systematically higher than those in the SPHnw simulation, and scatter in these central galaxy gas fractions (contributing scatter in SFR) is the largest factor driving higher σ_S for the SPHw case.

4   SHAM IN THE DM SIMULATION

So far we have applied subhalo abundance matching to the halo and subhalo hosts of galaxies in the SPH simulations, where the condensed baryons may improve the survival of dark matter substructures. We now turn to SHAM as it is traditionally applied by using the DM simulation, which starts from the same initial conditions but includes no baryons. Independent SO halos above the resolution limit have similar locations and masses in our SPHnw, SPHw and DM simulations. We identify dark matter substructures within these SO halos using the AdaptaHOP code as described earlier. While there is reasonable agreement in the number and abundance of subhalos between the two SPH simulations and the DM simulation, there are positional differences. For each subhalo above our resolution threshold of 64 particles, we trace its high redshift progenitors up to the epoch when it was an independent halo, i.e., up to z_{sat}.

The solid curve in each panel of Figure 7 shows the mean number of SPH galaxies per halo above a given stellar mass threshold in each halo mass bin in the SPHnw simulation. The four panels correspond to different stellar mass thresholds, and the mean space density of galaxies above these thresholds ranges from 0.004 to 0.06 $h^3\mathrm{Mpc}^{-3}$. The dashed curve shows the mean number of galaxies per halo when halos in the DM simulation are populated with galaxies using SHAM as described in §3, with a monotonic relation between stellar mass and M_H (equation 2). For comparison, the dotted curves show results of a model (SHAMz0) in which we assume a monotonic relationship between galaxy stellar mass and $z = 0$ subhalo mass, rather than z_{sat} subhalo mass. Note that the procedures of Vale & Ostriker (2004) and Weinberg et al. (2008) differ from SHAMz0 because they apply a global mass-loss correction to subhalo masses, though they do not consider post-z_{sat} mass loss on an object-by-object basis.

In low mass halos, where the satellite fraction is low, both the SHAMz0 and SHAM model predictions for the average number of galaxies per halo are in good agreement with the SPH simulation. At high halo mass, however, SHAMz0 underpredicts the number of galaxies per halo because it does not account for subhalo mass loss. The stellar masses assigned to subhalos are too low, and galaxies that should be above a stellar mass threshold instead fall below it. SHAM, on the other hand, remains in good agreement with the SPH simulation over a wide range of halo masses and galaxy stellar mass thresholds.

Figure 8 is the analogue of Figure 7, but using the SPHw simulation instead of the SPHnw simulation. As winds reduce stellar mass, the number density of galaxies above a given stellar mass threshold is lower than in the SPHnw simulation. Nonetheless, the trends for the SPHnw simulation discussed above still hold. Abundance matching using the $z = 0$ mass of subhalos underpredicts the number of galaxies in massive halos. Although, SHAM (using the z_{sat} mass of subhalos) provides a better fit to the SPH galaxy sample, it overpredicts the number of galaxies in massive halos to a larger degree than in the SPHnw simulation.

Figure 9 compares the halo occupations of SPH galaxies to the SHAM and SHAMz0 populations in each of the 30 most massive halos at $z = 0$, for galaxies above the 64 $m_{\mathrm{SPH}} = 5.8 \times 10^9 \mathrm{M}_\odot$ threshold. As already seen in Figures 7 and 8, SHAMz0 predicts too few galaxies in massive halos in both simulations. In the SPHnw simulation, the agreement between the number of SPH galaxies in each halo and the number of galaxies assigned to the halo by SHAM is remarkably good, indicating that SHAM is not just reproducing the typical number of galaxies for a given halo mass, but is also capturing the variation in galaxy number at a given halo mass. In the SPHw simulation, however, SHAM more noticeably overpredicts the number of galaxies in the most massive halos, and it does not track the variation in galaxy number at a given halo mass as well as in the SPHnw simulation.

Galaxy clustering depends on halo occupation statistics like those shown in Figures 7-9, and on small scales it also depends on the radial profile of satellites in massive halos. Figure 10 compares the radial number density profile of SPH galaxies around the central galaxy of the halo to the radial number density profile of galaxies assigned to halos

by SHAM and SHAMz0. The left panels correspond to the single most massive halo in the simulations, with $M_{\rm halo} = 4 \times 10^{14} {\rm M}_\odot$, while the right panels correspond to the three halos with $10^{14} {\rm M}_\odot < M_{\rm halo} < 3 \times 10^{14} {\rm M}_\odot$. In all cases, the slopes of the radial density profiles are similar for SPH galaxies and for subhalos populated by SHAM and by SHAMz0, but the normalisations and the inner truncations (indicated by where the curves stop) differ. The normalisation differences correspond to the differences in halo occupation at high $M_{\rm halo}$ seen in Figures 8 and 9. SHAMz0 predictions are always suppressed relative to SPH galaxies because they neglect subhalo mass loss. Tidal stripping is more severe for subhalos near the halo centre, exacerbating this effect and causing truncation of the SHAMz0 profiles at larger radii compared to SPH galaxies. Weinberg et al. (2008) found a similar truncation effect even when including a global correction for subhalo mass loss.

In contrast to SHAMz0, SHAM overpredicts the number of galaxies in high mass halos, by a small factor in the SPHnw simulation, and by 0.1-0.3 dex in the SPHw simulation. This overprediction is a consequence of neglecting stellar mass loss that occurs after $z_{\rm sat}$ in the SPH simulation, which is not accounted for in the SHAM recipe. The stellar mass loss is more severe for satellites close to the halo centre, so in this case the SPH profiles truncate at larger radii than the SHAM profiles.

This overprediction of satellite numbers may seem surprising in light of the good agreement between assigned and true stellar masses seen in Figure 2, with distributions that peak at $\log M_A/M_R = 0$ and have only mild asymmetry. However, the relations in Figure 2 (and the versions divided by halo mass in Figure 4) only include galaxies that remain above the 64 $m_{\rm SPH}$ stellar mass threshold at $z = 0$. Figure 11 plots M_S versus M_H for all satellites that lie above the resolution threshold *at the accretion epoch* $z_{\rm sat}$ in the wind simulation (lower panels), in parent halos with $z = 0$ mass $M_{\rm halo} > 10^{14} {\rm M}_\odot$ (left) and $10^{13.25} {\rm M}_\odot < M_{\rm halo} < 10^{14} {\rm M}_\odot$ (right). For the no-wind simulation, we adopt a higher stellar mass threshold of $2.9 \times 10^{10} {\rm M}_\odot$ so that the number of satellites is similar, enabling better visual comparison. In the high mass halos, a significant fraction of satellites have dropped below the mass threshold by $z = 0$ in the wind simulation, but SHAM would place all of these galaxies on the M_S-M_H relation traced by the bulk of the satellites. In the no-wind simulation, the fraction of satellites that suffer such severe mass loss is smaller. We suspect that galaxies in the wind simulation are more fragile because of their lower baryonic masses, and because they are typically less concentrated than galaxies formed without winds; in both respects, they more closely resemble observed galaxies. For intermediate mass halos, there are also galaxies that drop below the resolution threshold because of stellar mass loss, but the fractions are smaller.

Figure 12 shows the two-point correlation function of SPH galaxies (solid curve) and of halos and subhalos selected by SHAM (dashed curve) and by SHAMz0 (dot-dashed curve), in the SPHnw simulation (top) and the SPHw simulation (bottom). The space density of galaxies is 0.064 h^3 Mpc^{-3} in the SPHnw simulation and 0.018 h^3 Mpc^{-3} in the SPHw simulation, but we find qualitatively similar results at other stellar mass thresholds and space densities. SHAMz0 underpredicts the correlation function in both sim-

ulations, more severely for SPHw, as expected from its underpopulation of massive halos (Figures 7-10). At scales r $\geq 2 h^{-1}$Mpc, the "two-halo" regime of the correlation function, the depression of $\xi(r)$ reflects a drop in the galaxy bias factor from underweighting these highly biased halos. At scales $r \leq 1 h^{-1}$Mpc, where galaxy pairs within the same high mass halo make a large contribution, the suppression of $\xi(r)$ is more severe. For the SPHnw simulation, agreement between the SHAM and SPH-galaxy correlation functions is excellent, as one would expect from the close agreement of halo occupations and radial profiles seen in earlier figures. The largest discrepancies are 10% for both $2 h^{-1}$Mpc $< r \leq 10 h^{-1}$Mpc and $r \leq 2 h^{-1}$Mpc. For SPHw, the agreement in the 2-halo regime is still very good, with a maximum discrepancy of 15% for $2 h^{-1}$Mpc $< r \leq 10 h^{-1}$Mpc. However, the overpopulation of high mass halos leads to substantial overprediction of $\xi(r)$ in the 1-halo regime, by up to a factor of 2.5. As already discussed, this discrepancy arises from the severe stellar mass loss that affects a small but not negligible fraction of satellites in high mass halos and is not captured by the SHAM recipe. The impact on three-point or higher order correlation functions, which more strongly weight the single-halo occupations at small scales, would be more severe.

5 CONCLUSIONS

Ever since the identification of substructures in N-body simulations (e.g. Ghigna et al. 1998; Klypin et al. 1999; Moore et al. 1999; Springel et al. 2001), there have been efforts to associate them with galaxies (e.g. Colín et al. 1999; Kravtsov et al. 2004; Weinberg et al. 2008). Subhalo abundance matching (SHAM) has had impressive empirical success, reproducing observed galaxy clustering over a wide range of luminosity and redshift and correctly diagnosing (via cluster mass-to-light ratios) the overestimated matter clustering amplitude ($\sigma_8 \approx 0.9$ vs. $\sigma_8 \approx 0.8$) in WMAP1-era cosmological models (Conroy et al. 2006; Vale & Ostriker 2006; Guo et al. 2010; Moster et al. 2010). Our investigation provides the first full-scale test of SHAM against hydrodynamic cosmological simulations, where the correct identification between galaxies and subhalos is known a priori, including both a simulation with minimal feedback (SPHnw) and a simulation with momentum-driven winds that better reproduces the observed galaxy stellar mass function (Oppenheimer et al. 2010). This investigation yields physical insight into the galaxy formation process in these simulations, and it demonstrates the strengths and potential limitations of SHAM as a tool for interpreting observed galaxy clustering, significantly extending earlier studies by Nagai & Kravtsov (2005) and Weinberg et al. (2008).

When we consider galaxies above our adopted stellar mass threshold at $z = 0$, $M_S \geq 64\ m_{\rm SPH} = 5.8 \times 10^9\ {\rm M}_\odot$, we find a tight correlation between galaxy stellar mass and the mass of the parent halo or subhalo. For central galaxies, we consider the full mass of the spherical overdensity at $z = 0$, while for satellite galaxies we use the mass of the parent halo just before the epoch $z_{\rm sat}$ when it first becomes a satellite. Importantly, the median relation and scatter between M_S and M_H are similar for central galaxies and satellite galaxies, in both simulations, and the outlier fraction for satellite

galaxies is only modestly higher, mainly because of stellar mass loss in some satellites after z_{sat} . As a result, SHAM assignment of stellar masses is remarkably effective in both simulations. The 68% scatter in R = log M_A/M_R, where M_A is the assigned stellar mass and M_R the real (simulation) stellar mass, is $\sigma_M = 0.09$ dex for SPHnw and 0.11 dex for SPHw. The distribution of R is only mildly asymmetric, with a small extended tail of outliers. Similar results, with slightly increased scatter, hold at $z = 0.5$, 1 and 2. We find no clear correlation between residuals from the M_S-M_H relation and the satellite epoch at z_{sat} or the parent mass of the $z = 0$ halo, so our tests do not suggest a way to further tighten SHAM by considering additional properties.

Using R-band luminosity in place of stellar mass yields similar results, but with a larger population of outliers among satellites caused by their systematically older stellar populations and thus higher M_S/L ratios. SHAM should, therefore, be applied to stellar masses (estimated from luminosity and colour or spectral energy distribution) when possible. At $z = 2$, instantaneous star formation rates, which should be a good proxy for observed-frame optical luminosities, are well correlated with M_H, with similar correlations for central and satellite galaxies. SHAM assignment of star formation rates at this redshift is quite effective with a scatter in log $\text{SFR}_A/\text{SFR}_R$ of 0.12 dex in SPHnw and 0.16 dex in SPHw. This result reinforces empirical evidence, based on galaxy clustering data, that SHAM is an effective tool for modeling Lyman-break galaxies at high redshift.

SHAM is traditionally applied to N-body rather than SPH simulations (or to analytic descriptions calibrated on N-body). To test this standard form of SHAM, we have applied it to the AdaptaHOP subhalo population of a pure dark matter (DM) simulation started from the same initial conditions as the SPH simulations. Because subhalo positions within parent halos shift between SPH and DM (Weinberg et al. 2008), we have focused our comparison on halo occupation statistics and radial profiles, which together determine many properties of observable galaxy clustering, and on the real space two-point correlation function.

Using the galaxy stellar mass function of the SPHnw or SPHw simulation as input, SHAM (applied to the DM simulation) does quite well in reproducing the corresponding mean halo occupation, $< N(M_{\text{halo}}) >$, and the slope of the galaxy radial profile in high mass halos. In SPHnw, but not SPHw, SHAM traces the individual halo-to-halo variations in galaxy number at similar halo mass. Use of subhalo masses at z_{sat} rather than $z = 0$ makes a critical difference; if we use $z = 0$ subhalo masses, the galaxy occupation in high mass halos is systematically depressed because subhalos lose mass by tidal stripping after becoming satellites. Traditional SHAM (using z_{sat} masses), by contrast, tends to overpredict the galaxy numbers in high mass halos. We trace this discrepancy to the small but not negligible population of satellite galaxies that suffer severe stellar mass loss in the SPH simulations, so that they move from above our resolution threshold at z_{sat} to below it at $z = 0$. The subhalos themselves remain identifiable in the DM simulation, and SHAM populates them with galaxies that lie on the main M_S-M_H relation. The effect is more significant in the SPHw simulation, whose galaxies are apparently more vulnerable to severe mass loss because of their shallower baryonic potential wells. The mean occupation of high mass halos in SPHw is overpredicted by 0.1-0.3 dex, while in SPHnw the offset is less than 0.1 dex. For SPHnw, the SHAM-predicted correlation function agrees with that of SPH galaxies to better than 10% at all scales 0.05 h^{-1}Mpc $< r <$ 10 h^{-1}Mpc. For SPHw, SHAM predicts the correlation function to 15% at $r > 2$ h^{-1}Mpc but it overpredicts by a factor of ∼2.5 at $r < 0.5$ h^{-1}Mpc because of the overpopulation of massive halos.

In both of our SPH simulations, halo mass (at $z = 0$ for central galaxies or z_{sat} for satellite galaxies) is the primary determinant of galaxy stellar mass, luminosity, and (at high redshift) star formation rate. The most significant secondary factor, and thus the most significant limitation on the accuracy of SHAM, is the small fraction of satellite galaxies that suffer severe stellar mass loss even though their host subhalos survive. The sensitivity of feedback, indicated by the difference between our SPHnw and SPHw simulations, motivates further investigation of galaxy mass loss in high mass halos for a wider range of feedback prescriptions.

For galaxies with $L \geq L_*$, the SPHw simulation predicts excessive galaxy masses and excessive late-time star formation, indicating the need for an additional physical mechanism such as AGN feedback. The accuracy of SHAM for high luminosity galaxies will depend on how tightly correlated such feedback is with halo mass. Overall, however, the strong role of dark matter in governing galaxy formation makes subhalo abundance matching a powerful technique for making realistic artificial galaxy catalogues and for interpreting the observed distribution of galaxies.
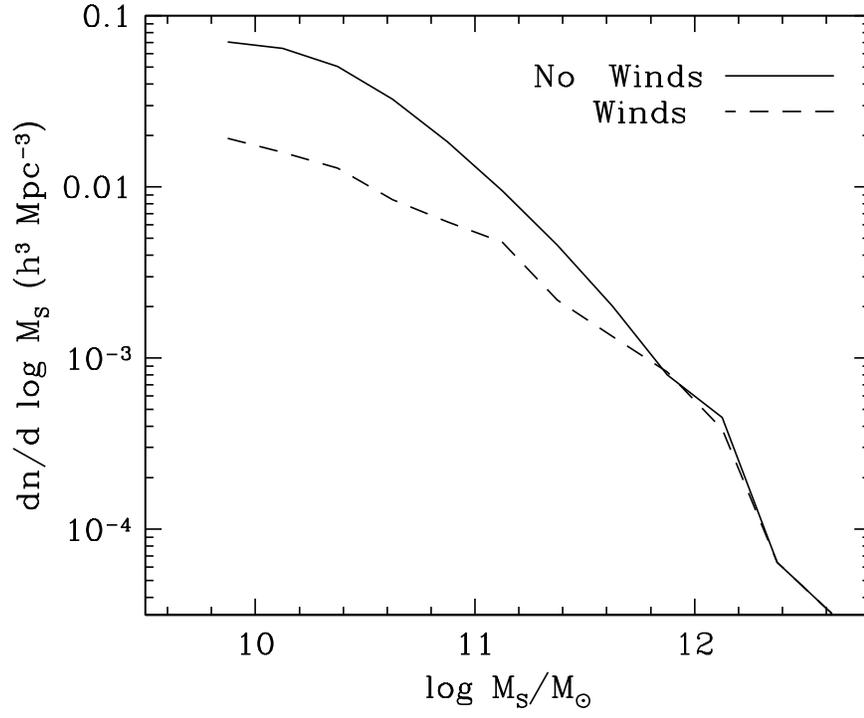
ACKNOWLEDGEMENTS

Figure 1. Galaxy stellar mass functions at $z = 0$ in the SPHw simulation (dashed), which incorporates momentum driven winds, and the SPHnw simulation (solid), which does not. In this and later plots, M_S refers to the stellar mass of SKID-identified galaxies.
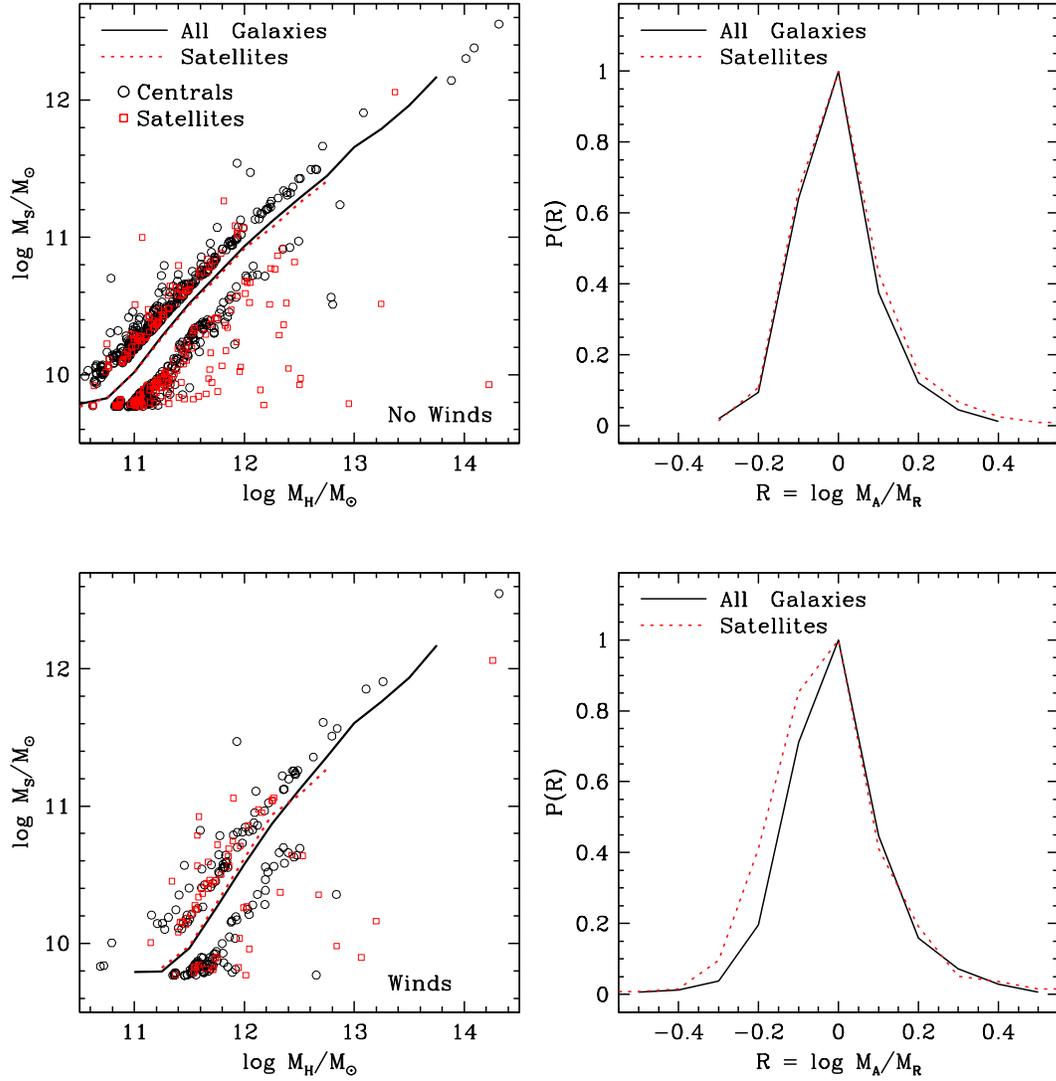
Figure 2. (Left) Stellar mass at $z = 0$ versus halo mass in the SPHnw simulation (top) and the SPHw simulation (bottom). Each point represents an SPH galaxy and we only include galaxies above the $M_S = 64 \, \mathrm{m_{SPH}} = 5.8 \times 10^9 \, \mathrm{M_\odot}$ threshold at $z = 0$. For central galaxies, shown as black points, the halo mass is the $z = 0$ mass of the host halo, while for satellite galaxies, shown as red points, the halo mass is the mass of the parent halo just before z_{sat}, the epoch at which it became a satellite. Only galaxies that are in the top 5% or bottom 5% by stellar mass in each 0.25 decade wide halo mass bin (relative to all galaxies in the bin) are shown. The solid and dotted curves show the median stellar mass in each halo mass bin for all galaxies and satellite galaxies respectively. (Right) Probability distribution of the ratio of stellar mass assigned by subhalo abundance matching to SPH galaxy mass in the SPHnw simulation (top) and SPHw simulation (bottom), with the solid curve standing for all galaxies and the dotted curve for satellite galaxies.
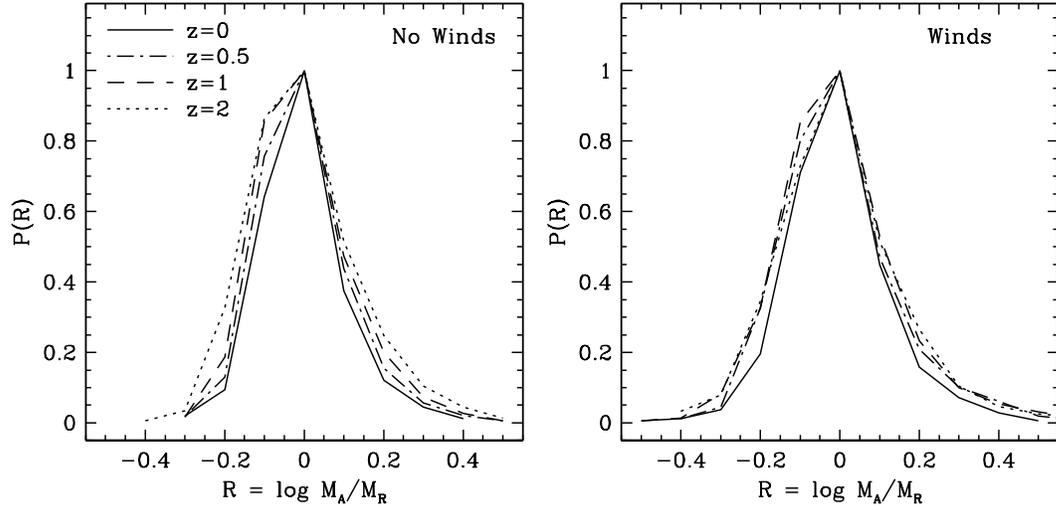
Figure 3. Probability distribution of the ratio of stellar mass assigned by subhalo abundance matching to SPH galaxy mass in the SPHnw simulation (left) and SPHw simulation (right). The solid, dot-dashed, dashed and dotted curves represent redshifts, $z = 0$, 0.5, 1 and 2 respectively.
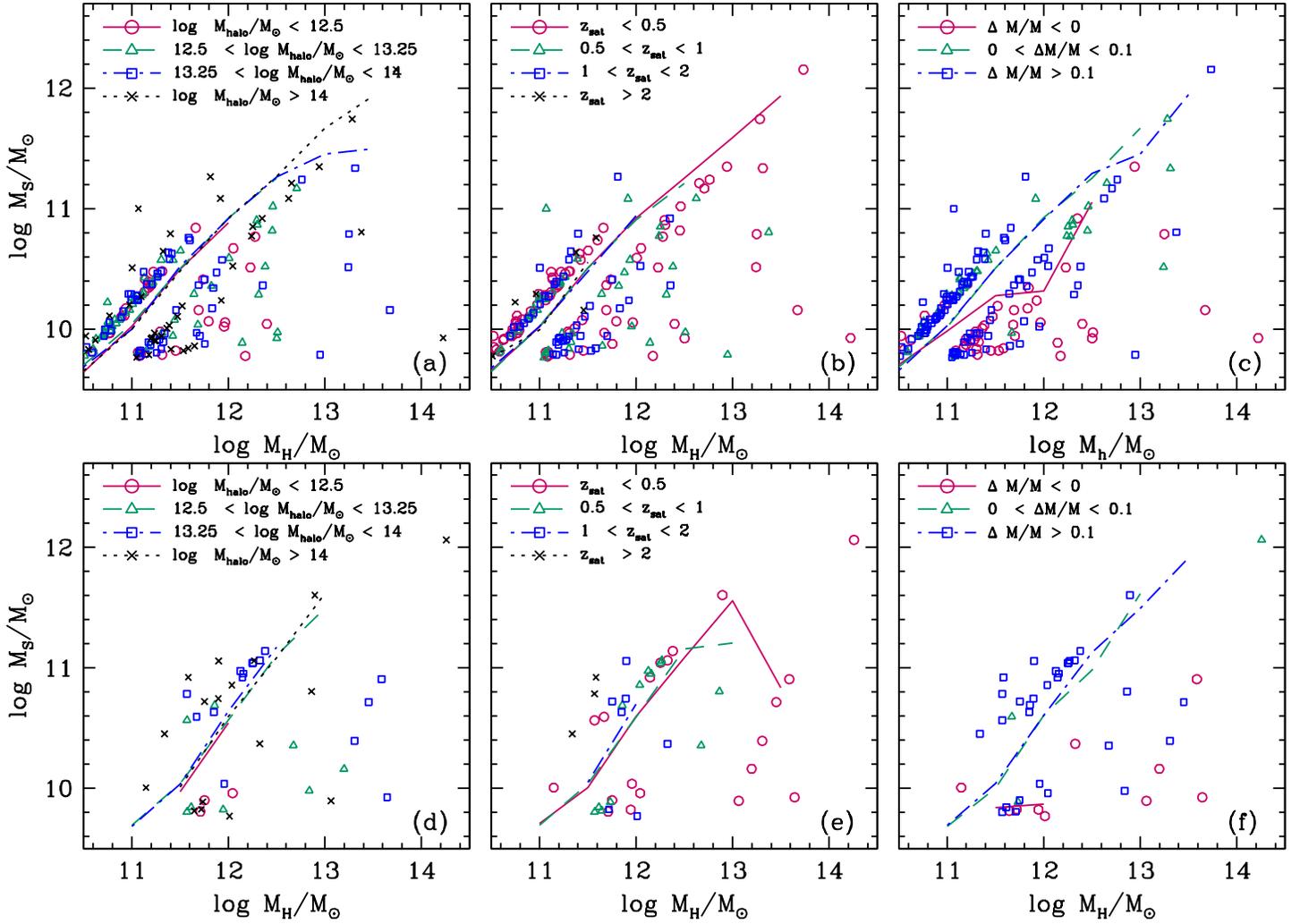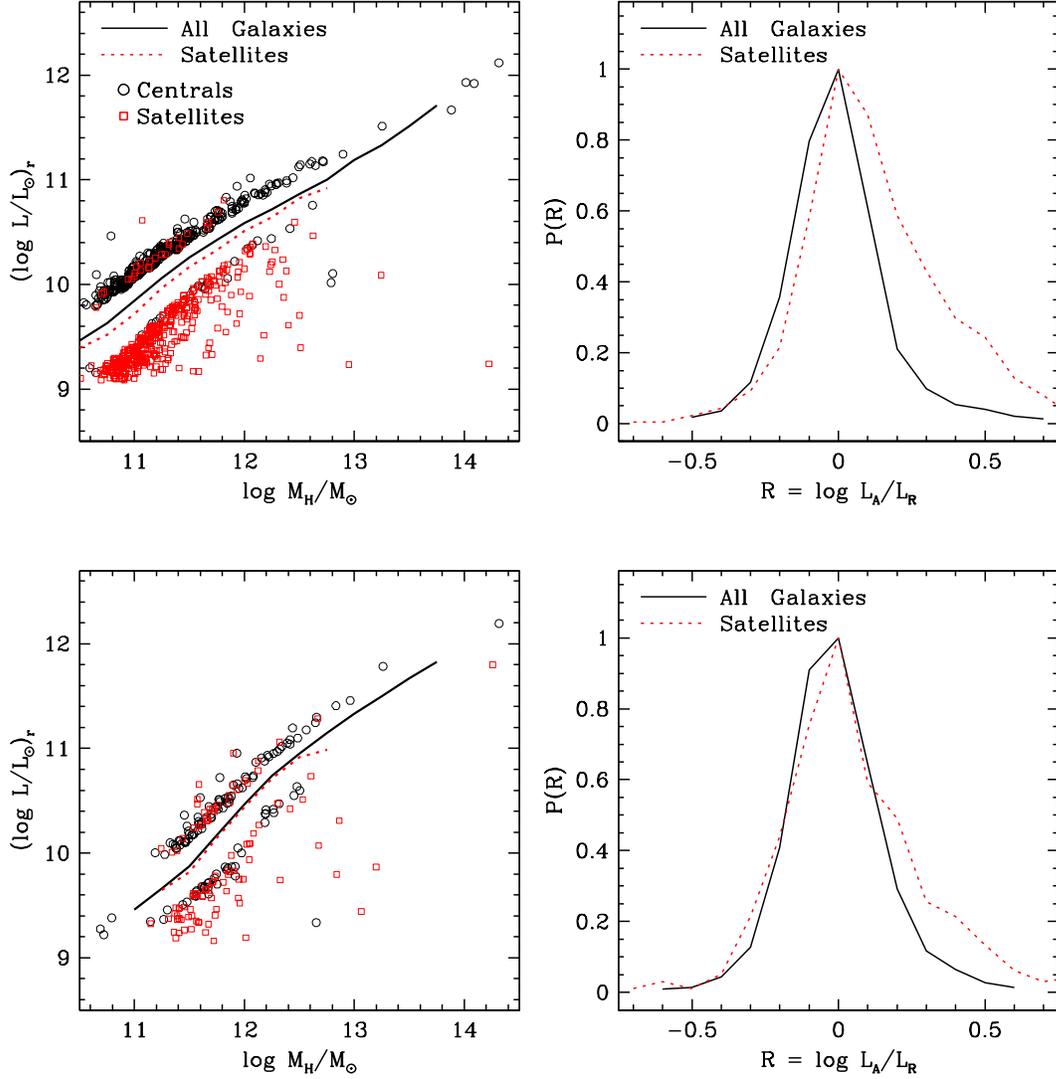
Figure 4. Stellar mass of satellite galaxies versus parent halo mass just before $z_{\rm sat}$. Each point represents a galaxy, and only galaxies that are in the top 5% or bottom 5% by stellar mass in each 0.25 decade wide halo mass bin (relative to the distribution of all galaxies) are shown. In panel (a), the circles, triangles, squares and crosses stand for different $z = 0$ host halo mass bins while in panels (b) and (c), they stand for bins of $z_{\rm sat}$, the epoch of accretion of the satellite and $\Delta M/M$, the change in stellar mass since $z_{\rm sat}$, respectively. Panels (d), (e) and (f) are analogous to panels (a), (b) and (c) but using the SPHw simulation.

Figure 5. (Left) *R*-band luminosity at $z = 0$ versus halo mass in the SPHnw simulation (top) and the SPHw simulation (bottom). Each point represents a galaxy in the SPHnw simulation. For central galaxies, shown as black points, the halo mass is the $z = 0$ mass of the host halo, while for satellite galaxies, shown as red points, the halo mass is the mass of the parent halo just before z_{sat}. Only galaxies that are in the top 5% or bottom 5% by *R*-band luminosity in each 0.25 decade wide halo mass bin are shown. The solid and dotted curves show the median *R*-band luminosity in each halo mass bin for all galaxies and satellite galaxies respectively. (Right) Probability distribution of the ratio of *R*-band luminosity assigned by subhalo abundance matching to *R*-band luminosity of SPH galaxies computed using a stellar population synthesis code in the SPHnw simulation (top) and SPHw simulation (bottom), with the solid curve standing for all galaxies and the dotted curve for satellite galaxies.
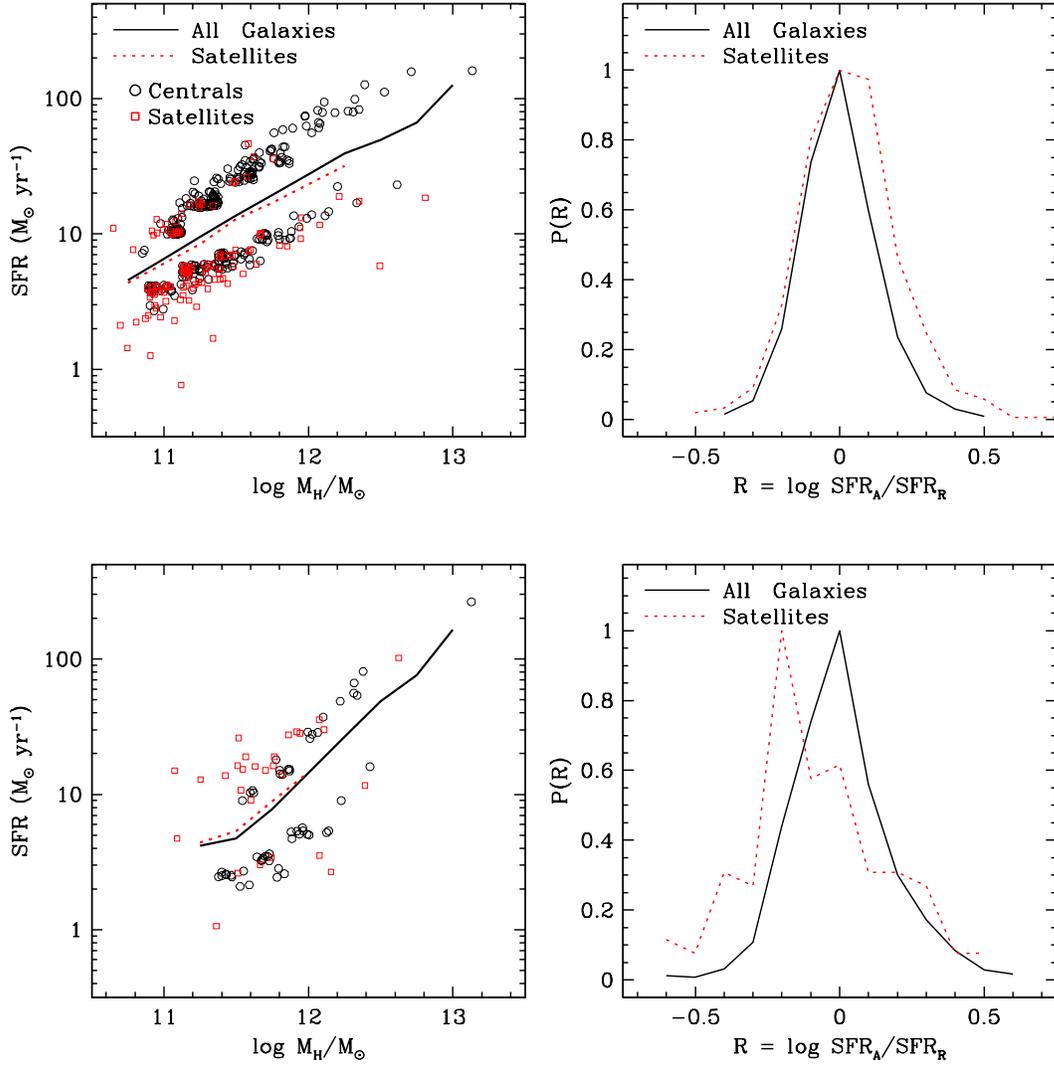
Figure 6. Relation between galaxy SFR and stellar mass (left), and accuracy of SHAM SFR assignment (right), for galaxies in the SPHnw (top) and SPHw (bottom) simulations at $z = 2$. The format is the same as Figures 2 and 5, but with instantaneous SFR used in place of stellar mass or R-band luminosity. Only galaxies with stellar mass above the 64 m_{SPH} threshold at $z = 2$ are included in the relations.
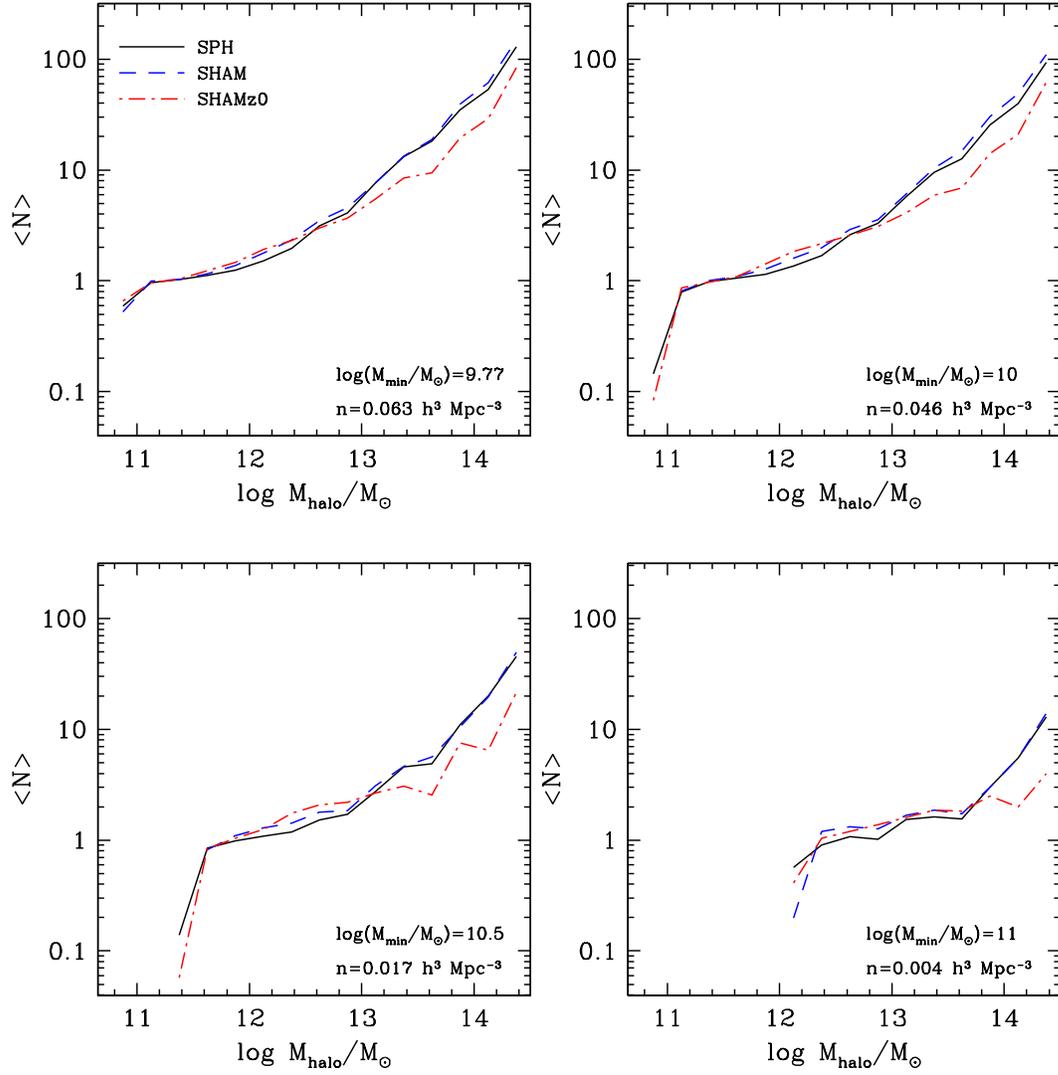
Figure 7. Mean number of galaxies per halo versus halo mass. The solid curve represents the SPHnw simulation, while the dashed and dotted curves are results from populating halos in our N-body simulation with galaxies using subhalo abundance matching (SHAM) with subhalo masses at z_{sat} and at $z = 0$ (SHAMz0), respectively. Each panel stands for a different galaxy stellar mass threshold, for which the corresponding space density of galaxies is also indicated.
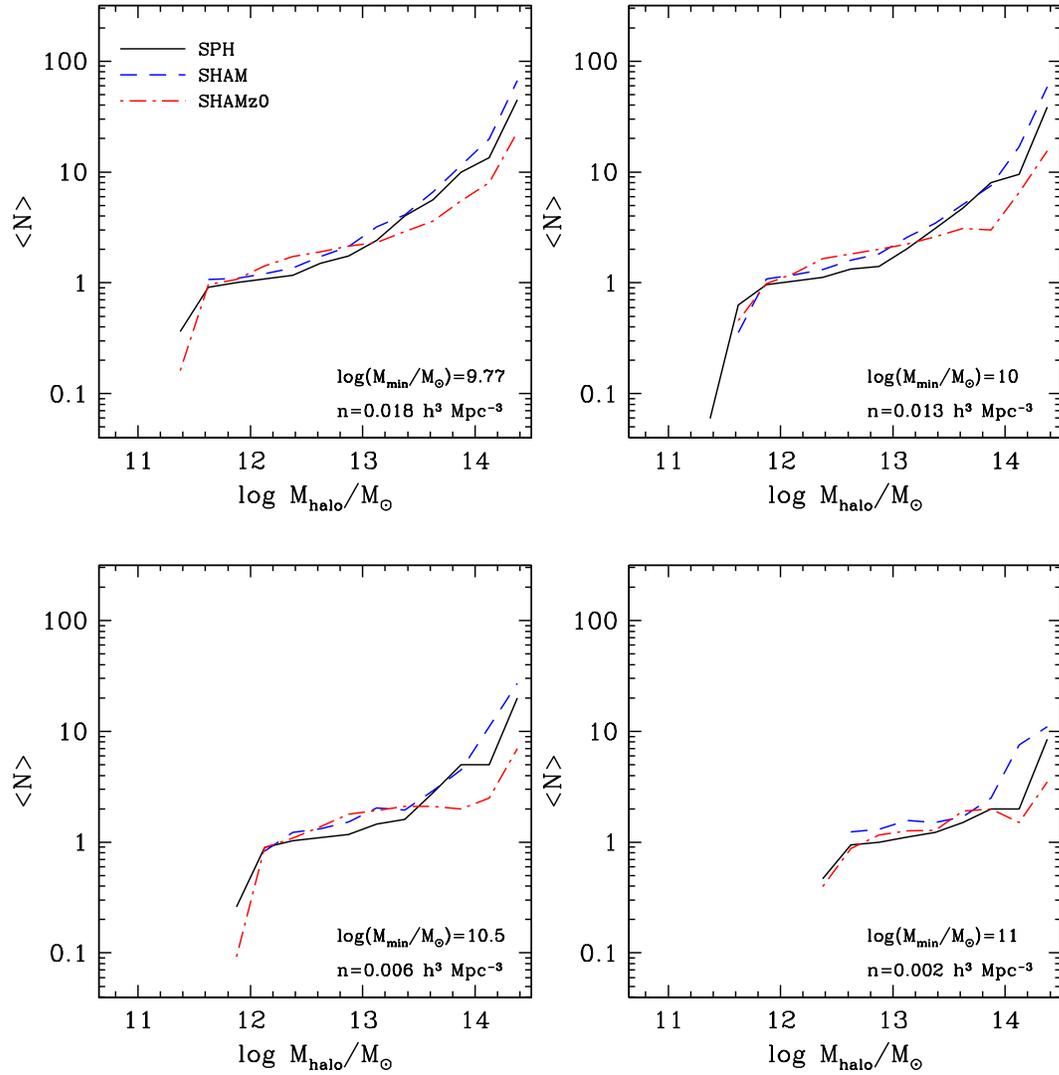
Figure 8. Mean number of galaxies per halo versus halo mass. This figure is analogous to figure 7 but using the SPHw simulation, which includes momentum driven winds.
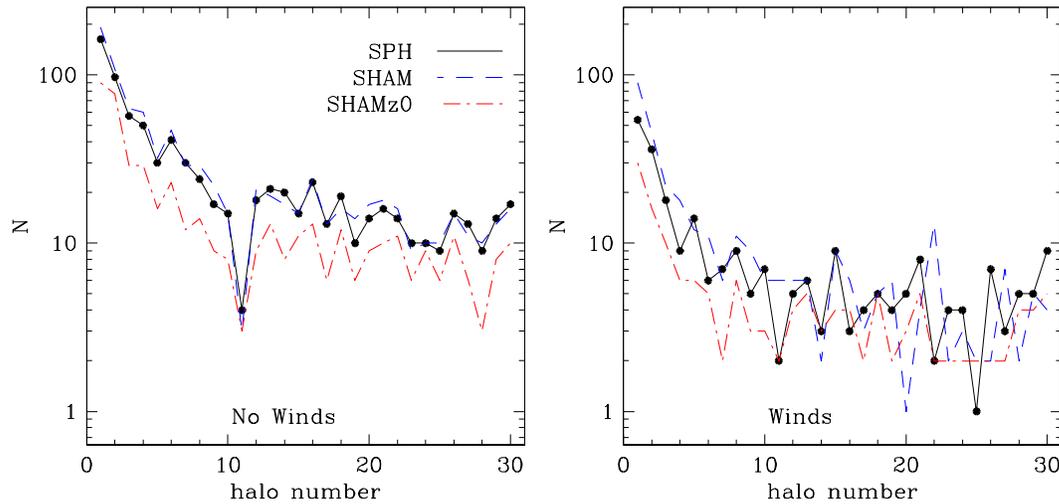

Figure 9. Halo occupations of the 30 most massive halos in the SPHnw (left) and SPHw(right) simulations. Points connected by the solid curve represent SPH galaxies, while the dashed and dotted curves represent SHAM and SHAMz0 respectively. All galaxies above the resolution threshold are included in this figure.
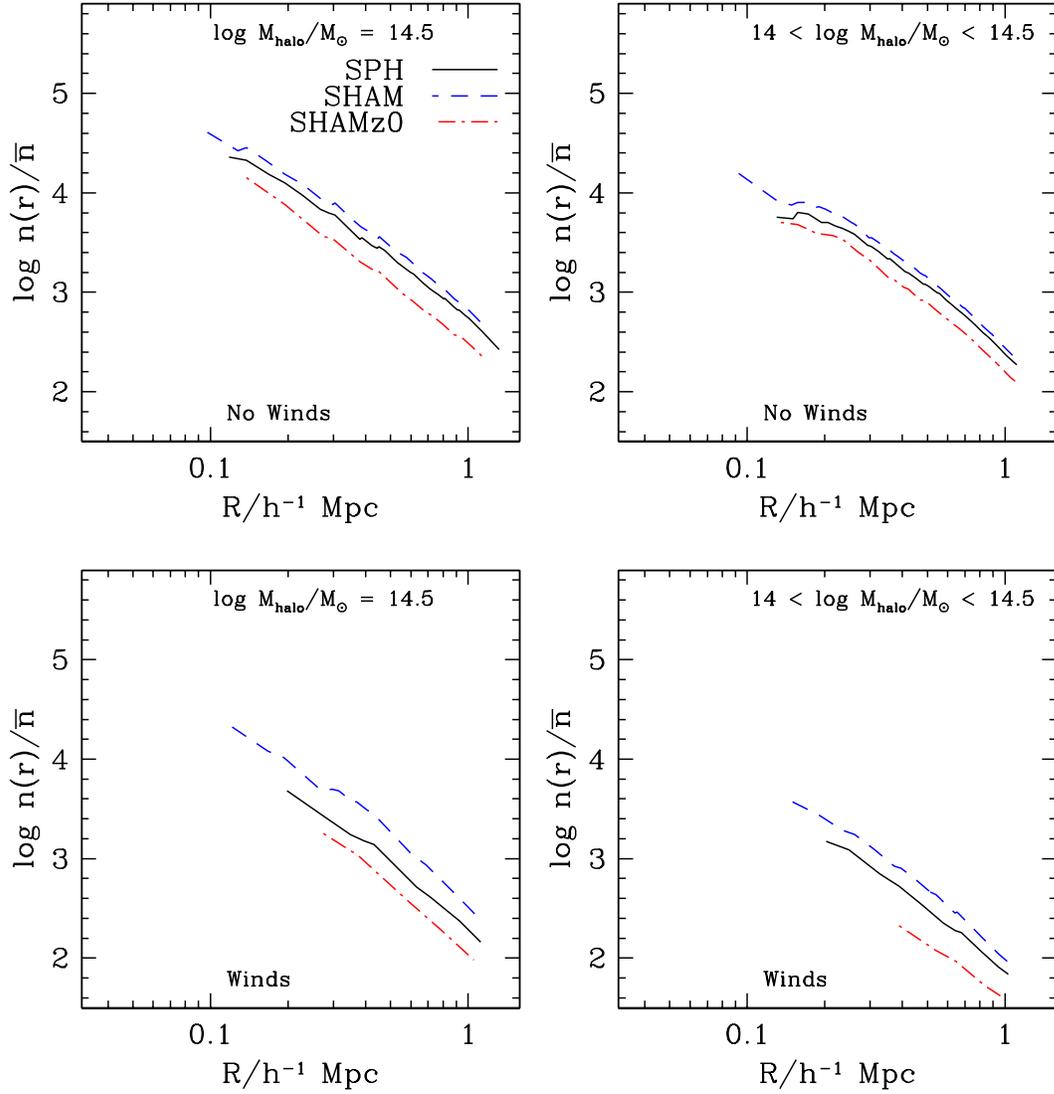
Figure 10. Radial number density profile of SPH galaxies (solid curve) and halos in the N-body simulation populated with galaxies using SHAM (dashed curve) and SHAMz0 (dot-dashed curve), for the mass threshold of $M_S = 5.8 \times 10^9$ $M_\odot$. The top two panels are for two halo mass bins in the SPHnw simulation while the bottom two panels are for two halo mass bins in the SPHw simulation. The curves stop when the only interior galaxy is the central galaxy.
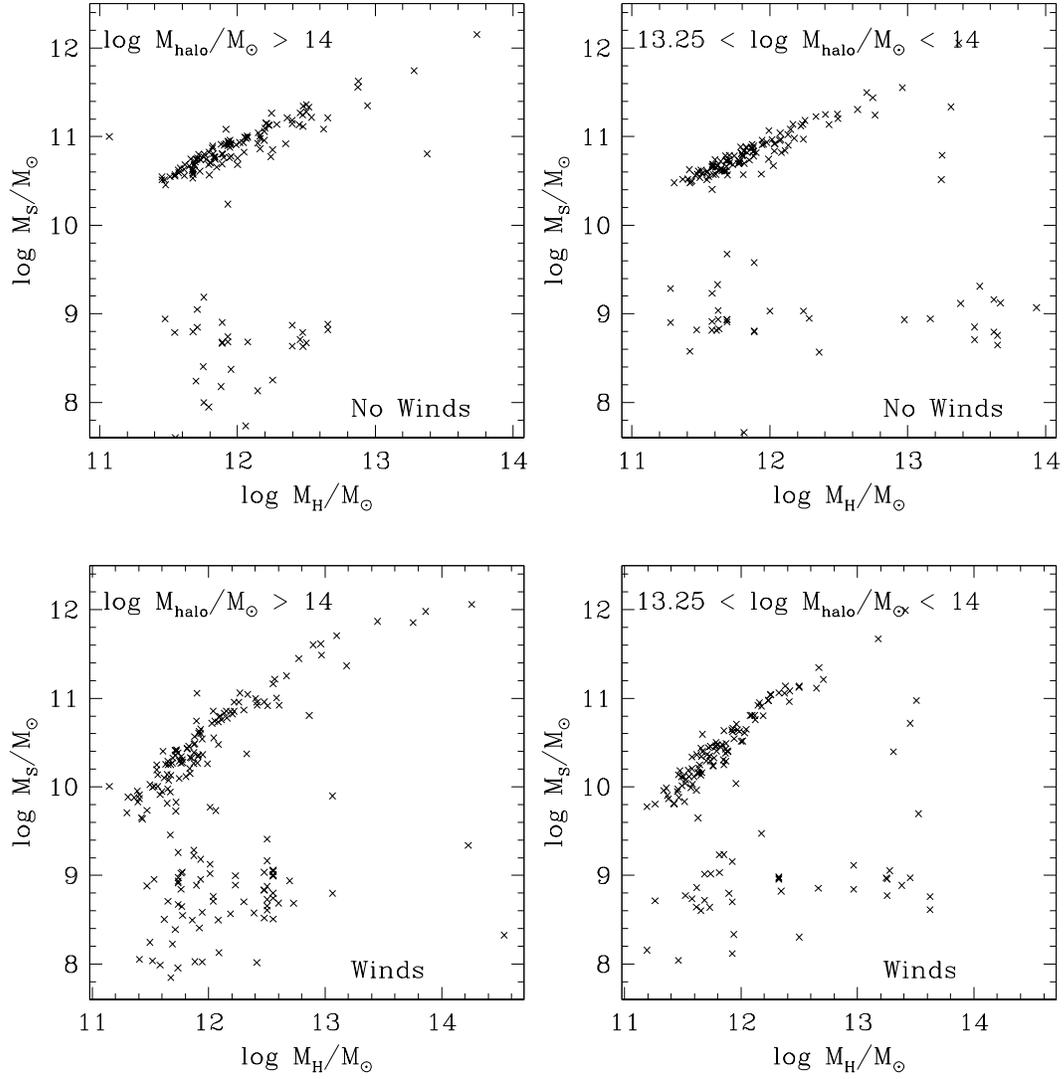
Figure 11. Stellar mass of satellite galaxies at $z = 0$ versus halo mass at $z_{\rm sat}$ in the SPHnw simulation (top) and the SPHw simulation (bottom). Each point represents a satellite galaxy above a stellar mass threshold at $z_{\rm sat}$ of 5.8×10^9 M$_\odot$ (SPHw) or 2.9×10^{10} M$_\odot$ (SPHnw), with the higher nw threshold chosen to yield a similar number of satellites. The left panels show galaxies that are located in halos above 10^{14} M$_\odot$, while the right panels show galaxies that are located in halos between $10^{13.25}$ M$_\odot$ and 10^{14} M$_\odot$.
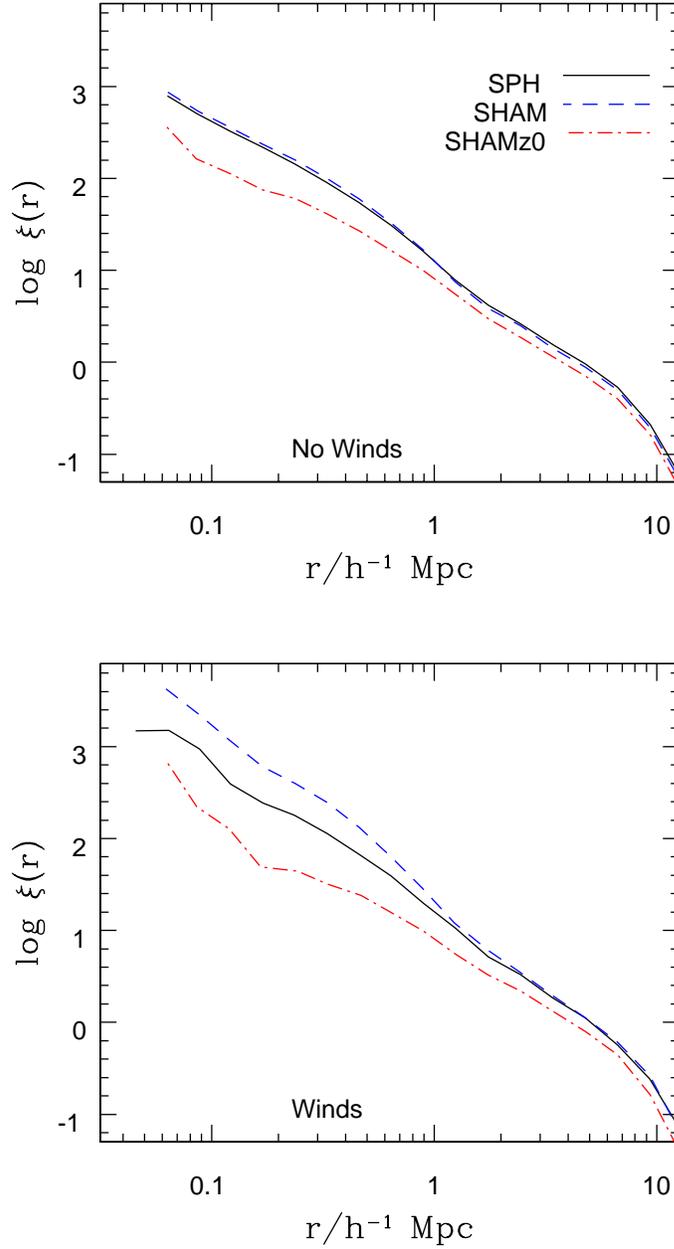
Figure 12. Two-point correlation function of SPH galaxies (solid curve) and halos and subhalos in the N-body simulation populated using SHAM (dashed curve) and SHAMz0 (dot-dashed curve). The top panel shows all galaxies above the resolution threshold in the SPHnw (no winds) simulation, and the bottom panel shows all galaxies above the resolution threshold (5.8×10^9 M$_\odot$) in the SPHw (winds) simulation.

REFERENCES

Aubert, D., Pichon, C., & Colombi, S. 2004, MNRAS, 352, 376

Barnes, J., & Hut, P. 1986, Nature, 324, 446

Berlind A. A., et al. 2003, ApJ, 593, 1

Conroy, C., Wechsler, R. H., & Kravtsov, A. V. 2006, ApJ, 647, 201

Conroy, C., & Wechsler, R. H. 2009, ApJ, 696, 620

Conroy, C., Gunn, J. E., & White, M. 2009, ApJ, 699, 486

Coles, P., Lucchin, F., Matarrese, S., & Moscardini, L. 1998, MNRAS, 300, 183

Colín, P., Klypin, A. A., Kravtsov, A. V., & Khokhlov, A. M. 1999, ApJ, 523, 32

Davis M., Efstathiou G., Frenk C. S., & White S. D. M. 1985, ApJ, 292, 371

Diemand, J., Moore, B., & Stadel, J. 2004, MNRAS, 352, 535

Evrard, A. E., Summers, F. J., & Davis, M. 1994, ApJ, 422, 11

Fall S.M., Efstathiou G. 1980, MNRAS,193,189.

Gao, L., White, S. D. M., Jenkins, A., Stoehr, F., & Springel, V. 2004, MNRAS, 355, 819

Gelb J.M., Bertschinger E. 1994, ApJ,436,467.

Ghigna, S., Moore, B., Governato, F., Lake, G., Quinn, T., & Stadel, J. 1998, MNRAS, 300, 146

Giavalisco, M., & Dickinson, M. 2001, ApJ, 550, 177

Guo, Q., White, S., Li, C., & Boylan-Kolchin, M. 2010, MNRAS, 404, 1111

Haardt, F., & Madau, P. 2001, Clusters of Galaxies and the High Redshift Universe Observed in X-rays,

Hernquist, L. 1987, ApJS, 64, 715

Hockney, R. W., & Eastwood, J. W. 1981, Computer Simulation Using Particles, New York: McGraw-Hill, 1981,

Katz N. 1992, PASP, 104, 852.

Katz N., Weinberg D. H., Hernquist L. 1996, ApJS, 105, 19.

Kazantzidis, S., Mayer, L., Mastropietro, C., Diemand, J., Stadel, J., & Moore, B. 2004, ApJ, 608, 663

Kereš, D., Katz, N., Fardal, M., Davé, R., & Weinberg, D. H. 2009, MNRAS, 395, 160

Kennicutt, R. C., Jr. 1998, ApJ, 498, 541

Klypin, A., Kravtsov, A. V., Valenzuela, O., & Prada, F. 1999, ApJ, 522, 82

Kravtsov, A. V., Berlind A. A., Wechsler R. H., Klypin A. A., Gottlöber S., Allgood B., Primack, J. R. 2004, ApJ, 609, 35

Larson, D., et al. 2010, arXiv:1001.4635, ApJ, in press

Li, C., & White, S. D. M. 2009, MNRAS, 398, 2177

Mandelbaum, R., Seljak, U., Kauffmann, G., Hirata, C. M., & Brinkmann, J. 2006, MNRAS, 368, 715

Mo, H. J., Mao, S., & White, S. D. M. 1999, MNRAS, 304, 175

Moore, B., Quinn, T., Governato, F., Stadel, J., & Lake, G. 1999, MNRAS, 310, 1147

Moster, B. P., Somerville, R. S., Maulbetsch, C., van den Bosch, F. C., Macciò, A. V., Naab, T., & Oser, L. 2010, ApJ, 710, 903

Murali C., Katz N., Hernquist L., Weinberg D. H., Davé R. 2002, ApJ, 571, 1

Nagai, D., & Kravtsov, A. V. 2005, ApJ, 618, 557

Oppenheimer, B. D., & Davé, R. 2006, MNRAS, 373, 1265

Oppenheimer, B. D., & Davé, R. 2008, MNRAS, 387, 577

Oppenheimer, B. D., Davé, R., Kereš, D., Fardal, M., Katz, N., Kollmeier, J. A., & Weinberg, D. H. 2010, MNRAS, 406, 2325

Reid, B. A., et al. 2010, MNRAS, 404, 60

Scannapieco, E., & Thacker, R. J. 2003, ApJL, 590, L69

Schmidt, M. 1959, ApJ, 129, 243

Simha, V., Weinberg, D. H., Davé, R., Gnedin, O. Y., Katz, N., & Kereš, D. 2009, MNRAS, 399, 650

Somerville, R. S., Primack, J. R., & Faber, S. M. 2001, MNRAS, 320, 504

Springel V., Yoshida N., White S. D. M. 2001, New Astronomy, 6, 79

Springel V., & Hernquist L. 2002, MNRAS, 333, 649

Springel, V., & Hernquist, L. 2003, MNRAS, 339, 289

Springel, V. 2005, MNRAS, 364, 1105

Steidel, C. C., Giavalisco, M., Dickinson, M., & Adelberger, K. L. 1996, AJ, 112, 352

Steidel, C. C., Adelberger, K. L., Giavalisco, M., Dickinson, M., & Pettini, M. 1999, ApJ, 519, 1

Steidel, C. C., Adelberger, K. L., Shapley, A. E., Pettini, M., Dickinson, M., & Giavalisco, M. 2003, ApJ, 592, 728

Kitayama, T., & Suto, Y. 1996, ApJ, 469, 480

Trujillo-Gomez, S., Klypin, A., Primack, J., & Romanowsky, A. J. 2010, arXiv:1005.1289, ApJ, in press

Vale, A., & Ostriker, J. P. 2004, MNRAS, 353, 189

Vale, A., & Ostriker, J. P. 2006, MNRAS, 371, 1173

Weinberg D.H., Colombi S., Davé R., Katz N. 2008, ApJ, 678, 6.

White S.D.M., Rees M.J. 1978, MNRAS 183,341.

Zheng Z., et al. 2005, ApJ, 633, 791

Zu, Y., Weinberg, D. H., Davé, R., Fardal, M., Katz, N., Keres, D., & Oppenheimer, B. D. 2010, arXiv:1005.4406, MNRAS, in press